# Redox-Mediated Pyrene Electrolytes for Enhancing the Reversibility of Vertically Arranged Tin Electrodes in Seawater Batteries

*Dowan Kim, Youngjae Jung, Wang-Geun Lee, Hyeon Seok Lee, Hyun Woo Kim, Jihun Cho, Seyoung Lee, Seohae Kim, Hyo Jin, Hyeji Min, Jin Bae Lee, Youngsik Kim, Stefano Passerini,* and Yongil Kim**

**Seawater batteries (SWBs) have emerged as a next-generation battery technology that does not rely on lithium, a limited resource essential for lithium-ion batteries. Instead, SWBs utilize abundant sodium from seawater, offering a sustainable alternative to conventional battery technologies. Previous studies have demonstrated the feasibility of achieving high energy densities in SWB anodes using vertically aligned electrodes. However, the use of tin anode materials with high volumetric energy density has encountered reversibility challenges due to the electrical isolation of tin particles caused by severe pulverization during charging and discharging. In this study, the reversibility of vertically arranged tin electrodes is improved by promoting desodiation of pulverized tin particles through the use of sodium-pyrene (Na-Pyr) as a redox mediator. The Na-Pyr redox-mediated electrolyte, combined with vertically aligned tin electrodes, demonstrates reversible capacities of 6 mAh $cm^{-2}$ over 80 cycles in SWBs. Furthermore, it is shown that arranging the electrodes vertically to maximize the area can achieve a high areal capacity of up to 40 mAh $cm^{-2}$. The combination of the Na-Pyr redox mediator and vertical tin electrode, with its excellent electrochemical performance, is promising as a practical anode material for enabling SWBs to achieve high energy density.**

## 1. Introduction

The advent of the Battery of Things era has brought about a significant change, i.e., the ability of electronic devices to be charged and utilized wirelessly.[1] This has resulted in a fundamental change in perspective, as evidenced by the projected growth of the electric vehicle and energy storage system industries, which will lead to a significant increase in the demand for lithium-ion batteries (LIBs), currently the predominant choice in battery systems.[2] Nevertheless, LIBs face significant challenges due to the high costs associated with lithium- and cobalt-based materials, as well as safety concerns regarding their use of flammable organic electrolytes.[3] Consequently, researchers are investigating alternative rechargeable battery systems that offer lower costs, greater sustainability, and enhanced safety compared to LIBs. This interest in alternative technologies has led to a focus on seawater batteries (SWBs), which utilize sodium ions from seawater instead of lithium ions.[4] SWB technology offers excellent thermal stability due to its water-in-battery structure, operating by immersion in seawater and providing a cooling effect.[5] The abundance of sodium ions in seawater provides an almost limitless resource for the sodium element, facilitating its use in rechargeable sodium ion batteries. The high theoretical energy density of SWBs (3051 Wh $L^{-1}$) is attributed to the ability to store the sodium source in

D. Kim, Y. Jung, W.-G. Lee, H. S. Lee, J. Cho, S. Lee, S. Kim, H. Jin, H. Min, Y. Kim
School of Energy & Chemical Engineering
Ulsan National Institute of Science and Technology (UNIST)
UNIST-gil 50, Ulsan 44919, Republic of Korea

H. W. Kim, J. B. Lee
Research Center for Materials Analysis
Korea Basic Science Institute (KBSI)
Daejeon 34133, Republic of Korea

S. Passerini
Helmholtz Institute Ulm (HIU)
Helmholtzstrasse 11, 89081 Ulm, Germany
E-mail: stefano.passerini@kit.edu

S. Passerini
Karlsruhe Institute of Technology (KIT)
P.O. Box 3640, 76021 Karlsruhe, Germany

S. Passerini
Austrian Institute of Technology
Giefinggasse 4, Wien 1210, Austria

Y. Kim
School of Chemical
Biological and Battery Engineering
Gachon University
Seongnam-si, Gyeonggi-do 13120, Republic of Korea
E-mail: yikim@gachon.ac.kr

the anode through the use of external ambient seawater as the cathode.[6]

Although SWBs have a high theoretical energy density, their practical energy density is low due to the structural limitations of the present system. The cell structure of SWBs consists of three main components. First, the cathode part contains seawater and cathode current collectors such as Ti mesh and carbon cloth.[7] Second, there is a solid electrolyte termed a NASICON (Na super ionic conductor) ceramic, which physically separates the cathode and anode.[8] Finally, the anode part has a specific layout, consisting of a single-sided stainless steel (SUS) frame in a coin cell.[9] This anode part is filled with liquid electrolyte and anode materials. Consequently, the capacity to store energy in the restricted anode area is a critical factor in determining the energy density of SWBs. Two methods have been proposed to achieve high energy density of the conventional anode: 1) utilizing active materials with inherent high energy density,[10] and 2) maximizing the loading of active materials in the anode.[11] Anode materials with high energy density are typically those relying on an alloying mechanism, such as red phosphorus[12] (2596 mAh $g^{-1}$) and tin[13] (847 mAh $g^{-1}$). However, they had the disadvantage of poor cycle life characteristics due to pulverization, caused by extreme changes in volume during cycling.[14] This issue was particularly evident during desodiation on alloying-type anodes, as evidenced by previous studies that had demonstrated a larger delithiation/desodiation polarization of alloying-type anodes than the lithiation/sodiation polarization.[15] Another proposal for achieving high energy density involved maximizing the loading of active material, which could be achieved in a straightforward manner by filling the anode space with a thick electrode structure. However, this proved challenging due to the limitations of present electrode manufacturing technology, specifically the slurry coating process on metal foil collectors. This process led to low mechanical stability, including issues such as delamination and cracking.[16] In order to address the difficulties associated with thick electrodes, comprehensive investigations were conducted into vertical electrode configurations.[17] The vertical arrangement facilitated fast ion transport, even with a thick electrode, due to its low tortuosity.[18] This arrangement greatly enhanced the electrochemical efficiency of the thick electrode. Previous work[19] demonstrated that vertically oriented conventional anode-coated electrodes resulted in advantages for SWBs without any mechanical issues. Nevertheless, a significant issue when using alloying-type materials with high theoretical capacity remained the aforementioned electrical isolation between pulverized particles during cycling. This issue proved particularly problematic when vertical electrodes were employed, as such arrangements lacked the mechanical stability necessary to hold the separated particles and maintain the electrode structure.

The present study successfully improved the reversibility of a vertically aligned alloy-type anode, tin electrode, by utilizing a sodium-pyrene (Na-Pyr) redox mediator. The redox-mediated Na-Pyr enables a charge transfer reaction even on electrically isolated tin particles during desodiation, allowing capacity retention even in the presence of pulverized tin particles.[20] Our findings demonstrate that combining redox-mediated pyrene-based electrolytes with vertically arranged tin electrodes can enable high areal capacity anodes for sodium-based batteries, particularly SWBs.

## 2. Results and Discussion

### 2.1. Characterization of Pyrene Redox-Mediated Electrolyte

**Figure 1a** illustrates the charge transfer reaction between tin particles as a result of the redox reaction of the Na-Pyr. The pyrene-based redox-mediated electrolyte facilitates the oxidation of sodiated tin particles during the desodiation process, even when the tin particles are electrically isolated. During the desodiation process, significant polarization occurs as Na-Pyr undergoes desodiation to form Pyr, which then reacts with sodiated tin and facilitates its desodiation through a chemically driven mechanism. The desodiation of tin leads to significant polarization, caused by the volume expansion and pulverization that occurred during the prior sodiation process. At this point, Na-Pyr undergoes desodiation to produce Pyr, which then interacts with sodiated tin, enabling its desodiation through a chemically driven mechanism (Figure S1, Supporting Information).[21] Previous report[22] have demonstrated that sodium-polycyclic aromatic compounds form sodium cation-radical anion complexes with intrinsic electronic and ionic conductivity, and that there is a relationship between the reaction voltages depending on the polycyclic aromatic compound. The redox potential peaks for biphenyl (Bp), naphthalene (Nap), phenanthrene (Phe), and pyrene (Pyr) have been identified at 0.095 V ($Bp/Bp^{\bullet-}$), 0.154 V ($Nap/Nap^{\bullet-}$), 0.224 V ($Phe/Phe^{\bullet-}$), and 0.621 V ($Pyr/Pyr^{\bullet-}$), respectively. These materials have a tendency to bind free radicals, thereby facilitating the transfer of an electrical charge.[23] The presence of unpaired electrons can be identified through the Dysonian peak observed in electron paramagnetic resonance spectroscopy (Figure 1b).

Prior to evaluating the electron transfer ability of Na-Pyr, its composition was validated by conducting a solubility assessment in diethylene glycol dimethyl ether (DEGDME) (Figure S2a, Supporting Information). The concentration of Pyr was gradually increased from 0.1 M to 0.8 M, and after 24 h, Pyr precipitates were observed. The solution remained transparent at concentrations ranging from 0.1 M to 0.5 M; however, at concentrations above 0.6 M, the formation of Pyr precipitates was evident. Subsequently, an excess of Na metal was added to produce unpaired electrons, resulting in the formation of Na-Pyr (as seen in Figure S2b, Supporting Information).

In order to determine the suitability of Na-Pyr as a redox mediator for tin anodes, a comparison was conducted between the reaction voltages of tin using galvanostatic charge–discharge tests (Figure 1c). A half-cell utilizing Na metal as the counter electrode was employed to compare the voltage profiles of the second sodiation–desodiation cycle. Tin exhibited a discharging reaction at voltages below 0.7 V, whereas Na-Pyr exhibited a reaction within a voltage of 0.7 V. This was further confirmed by the differential capacity plot shown in Figure 1c. During the tin desodiation process, two major reactions were observed at 0.14 and 0.27 V, with additional reactions at 0.53 and 0.62 V. In comparison, the Na-Pyr desodiation potential was observed at 0.68 V, indicating that the redox reaction potential of Pyr is significantly higher than that of tin desodiation. Therefore, Na-Pyr can be considered a suitable redox mediator for the tin anode. During the desodiation of sodiated tin, the pulverized and electrically

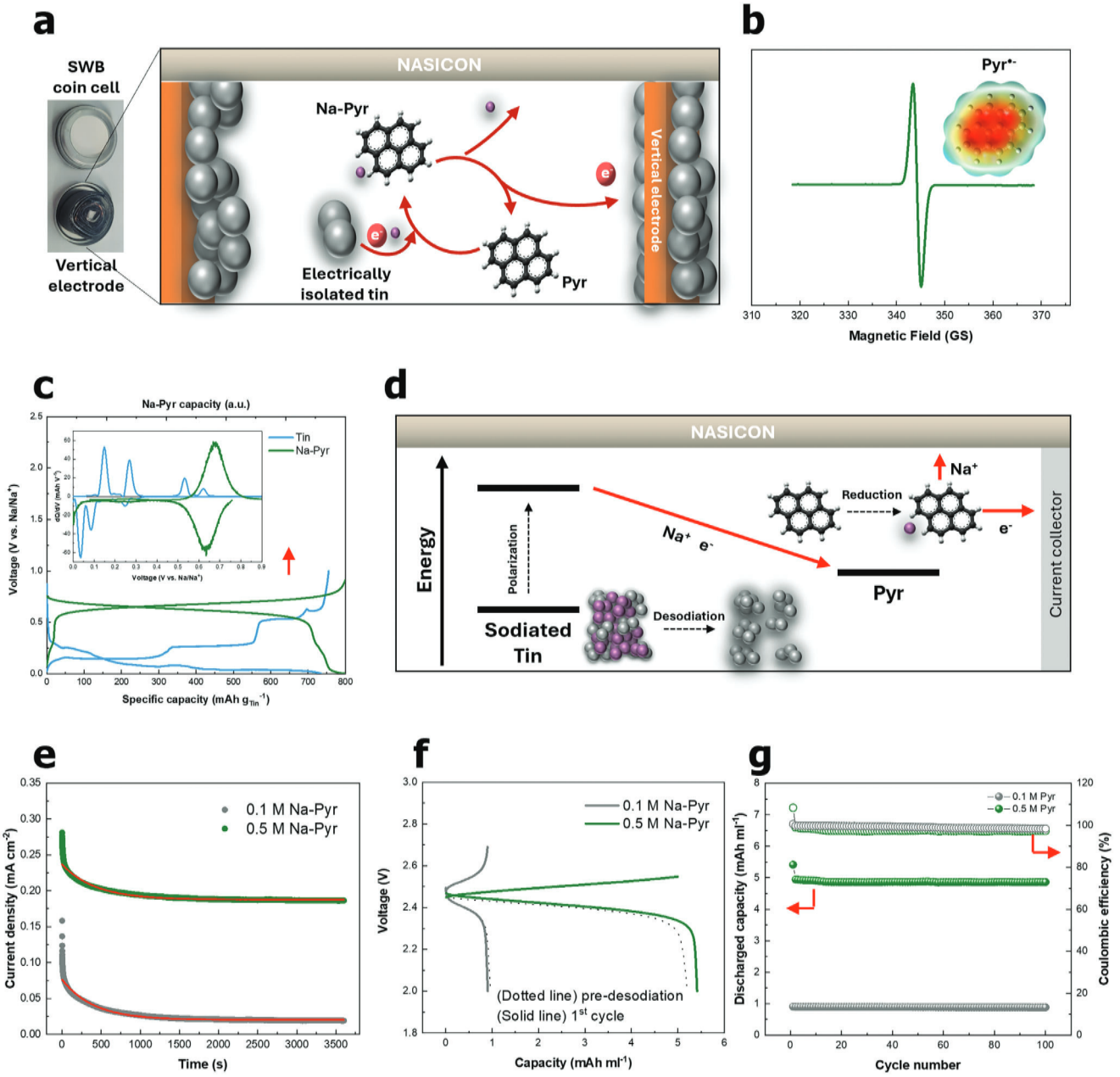


**Figure 1.** a) The illustration shows the role of redox-mediated Na-Pyr to electrically isolated tin particles. b) EPR spectra of Na-Pyr. c) The voltage profile during charging–discharging of tin and Na-Pyr in a half-cell with a counter electrode made of Na metal foil. The corresponding differential capacity plot is also included. d) A diagram of the energy levels in the desodiation process of sodiated tin and the redox reaction of the Na-Pyr. e) The ITIC curves and their fitting lines for a solution of 1 M $NaPF_6$ in DEGDME with either 0.1 M Na-Pyr or 0.5 M Na-Pyr redox mediator. f) The galvanostatic charge–discharge voltage curve for an electrolyte containing either 0.1 M Na-Pyr or 0.5 M Na-Pyr redox mediator, and g) their cyclabilities.

isolated tin undergoes significant polarization due to volume expansion and reduced contact area. In the presence of Na-Pyr, the Na-Pyr is first desodiated (oxidized), and the oxidized Pyr then chemically oxidizes the sodiated isolated tin, enabling reversible capacities. In this process, the electron transfer limitations caused by the limited contact area between the tin particles and electrically isolated tin particles are mitigated by the liquid state of Na-Pyr (Figure 1d).

The Na-Pyr redox-mediator electrolyte was prepared by combining the produced Na-Pyr with a 1 M sodium hexafluorophosphate ($NaPF_6$) in a DEGDME solution, which is a commonly used conventional electrolyte (CE).[24] The isothermal transient ionic current (ITIC) method[25] was employed to independently verify the ionic and electronic conductivity of the 0.1 M and 0.5 M concentrations of Na-Pyr redox-mediator electrolyte (Figure 1e). A voltage was applied across two stainless steel electrodes

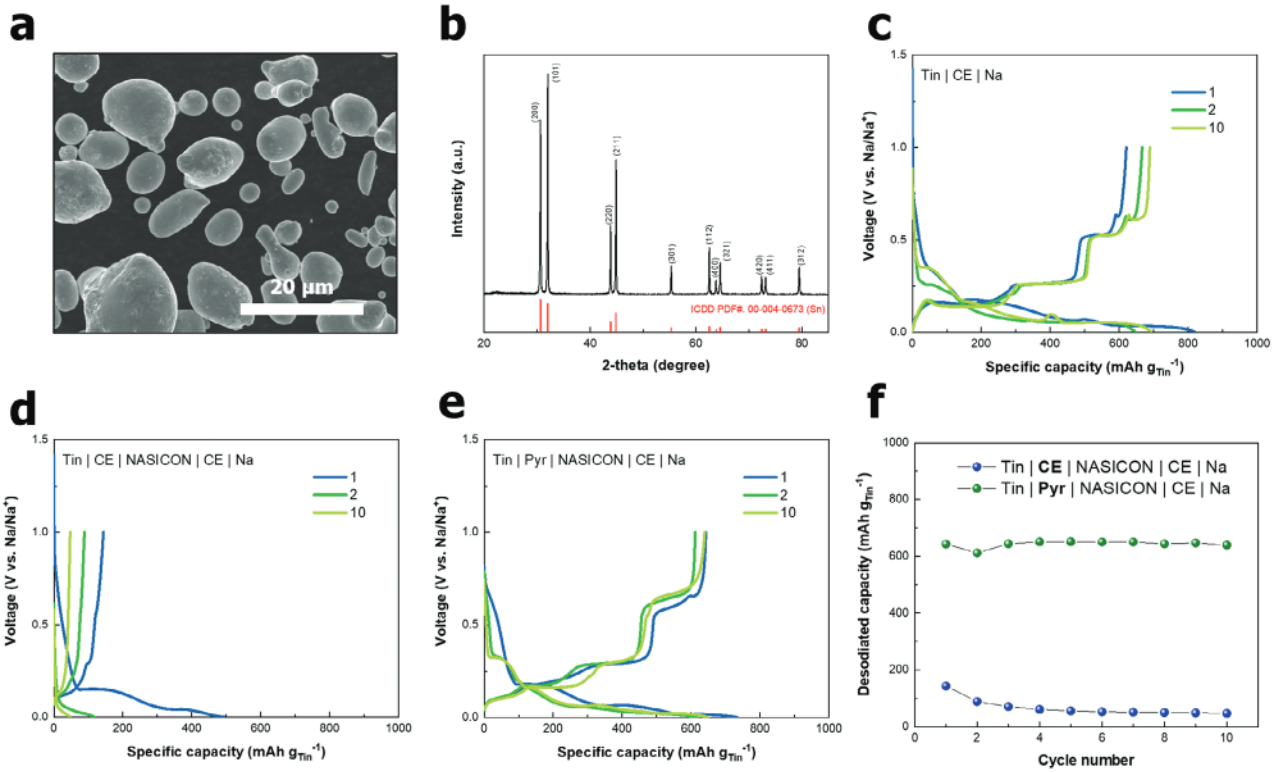


**Figure 2.** a) SEM image and b) XRD pattern of the tin powder. c) Voltage profile during galvanostatic charging–discharging of the tin anode in the half cell using Na metal foil as the counter electrode. Voltage profile during galvanostatic charging–discharging of the tin anode in the NASICON solid electrolyte-inserted half-cell with the d) conventional electrolyte and e) Na-Pyr redox-mediator electrolyte, and f) their respective cyclabilities.

(Figure S3, Supporting Information) containing 0.1 M or 0.5 M Na-Pyr redox-mediator electrolytes, and the resulting current was measured over time.

$$J\ (t) = \frac{\sigma_{dc,e^-}\ U}{d} + \frac{\sigma_{dc,Na^+} U}{d} exp\left(-\frac{\mu_{Na^+} U}{d^2} t\right) \quad (1)$$

The current density is determined as a function of time in the equation, J(t), where the electrolyte's electronic and ionic conductivities are denoted by $\sigma_{dc,e-}$ and $\sigma_{dc,Na+}$, respectively. The abbreviation U represents the applied voltage in the system, whereas $\mu N_{a+}$ denotes the mobility of $Na^+$ ions. Equation (1) showed that the electrolyte with 0.1 M Na-Pyr redox-mediator electrolyte exhibited electronic and ionic conductivities of 0.26 and 2.29 mS cm$^{-1}$, respectively, whereas the electrolyte with 0.5 M Na-Pyr redox-mediator electrolyte demonstrated conductivities of 2.46 and 1.88 mS cm$^{-1}$ (Table S1, Supporting Information). When considering only the ionic conductivities, the electrolyte containing 0.1 M Na-Pyr redox mediator demonstrated slightly higher conductivity compared to that with 0.5 M Na-Pyr redox mediator. However, the 0.5 M Na-Pyr electrolyte exhibited higher electronic conductivity, which is more advantageous for charge transfer according to the Na-Pyr redox-mediator concept.

The reversibility of the sodiation and desodiation processes in the Na-Pyr redox-mediator electrolyte was investigated to determine whether Na-Pyr can conduct a charge transfer reaction to tin particles without itself degrading (Figure 1f,g). In this experiment, Na-Pyr was employed not as a redox mediator but as an anode material. Through this experiment, we confirmed the reversibility of the Na-Pyr material during the redox reaction process, thereby demonstrating the potential of Na-Pyr to facilitate charge transfer through redox reactions in a reversible manner as a redox mediator. The seawater coin-cell system utilized a catholyte comprised of a sodium ferrocyanide aqueous solution (Figure S4, Supporting Information).[26] The discharge capacities were measured as ≈1 and 5 mAh ml$^{-1}$ for electrolytes with 0.1 M and 0.5 M Na-Pyr, respectively. These measurements were taken at a current of 0.3 mA cm$^{-2}$, as indicated by the dotted line in Figure 1f. The subsequent analysis of the voltage profiles of the charging and discharging operations is indicated by the solid line in Figure 1f and Figure S5 (Supporting Information). Following several charge–discharge cycles, both electrolytes (0.1 M and 0.5 M Na-Pyr redox mediator) demonstrated stable discharged capacities for >100 cycles (Figure 1g; Figure S5, Supporting Information). The capacity retention of hundredth discharged capacities was 98.3% and 97.3%, respectively. This demonstrates that Na-Pyr serves as an effective redox mediator with excellent cycle stability.

### 2.2. Verification of Enhanced Cyclability in the Tin Electrode with Na-Pyr Redox-Mediator Electrolyte

**Figure** 2a,b presents scanning electron microscopy (SEM) and X-ray diffraction (XRD) investigations of tin particles utilized as

the anode active material. In previous studies, nano-sized tin or composite materials such as carbon were used to preserve the alloying anode particles' structure in order to compensate for the particles' volume expansion and pulverization.[27] In contrast to the methodology employed in previous studies, this investigation utilized micro-sized bare tin powder as the anode material. The use of micro-sized tin is advantageous due to its reduced synthesis costs, which render it highly suitable for industrial applications.[28] Additionally, the lower specific surface area of micro-sized materials minimizes their contact area with the electrolyte, which can help reduce electrolyte decomposition and improve overall cell stability.[29] The SEM images (see Figure 2a; Figure S6, Supporting Information) revealed significant variation in the sizes of tin particles, ranging from a few micrometers to tens of micrometers. After fabricating the electrodes using micro-sized tin particles and assembling them into half-cell using Na metal foil as the counter electrode, sodiation and desodiation were performed at a current density of 0.13 mA $cm^{-2}$ (Figure 2c). The desodiation capacity of the second cycle was 667 mAh $g_{Tin}^{-1}$, and that of the tenth cycle was 689 mAh $g_{Tin}^{-1}$. These results are, respectively, ≈21.3% and 18.7% lower than the theoretical capacity of tin, which is 847 mAh $g^{-1}$.[30] To investigate the potential of the Na-Pyr redox reaction in enhancing the cyclability of the tin electrode through electron transfer between particles, we constructed a coin cell consisting of a NASICON solid electrolyte integrated into the conventional Na metal half-cell structure. Subsequently, the cyclability of the conventional electrolyte and the Na-Pyr redox-mediator electrolyte was compared. To operate the cell with the NASICON inserted, we used 2464 coin cells instead of the standard 2032 coin cells to accommodate the space required for the NASICON layer. However, the increased height of the 2464 coin cell made it challenging to apply sufficient internal pressure using the spring. This issue resulted in the initial desodiation capacity[31] of the cell employing the conventional electrolyte and NASICON being only 143 mAh $g_{Tin}^{-1}$, further decreasing to 88 mAh $g_{Tin}^{-1}$ in the second cycle and 45 mAh $g_{Tin}^{-1}$ in the tenth cycle. In contrast, the combination of tin and the Na-Pyr redox-mediator electrolyte together with NASICON (Figure 2e) demonstrated more stable performance, maintaining a consistent desodiation capacity of 643 mAh $g_{Tin}^{-1}$, 612 mAh $g_{Tin}^{-1}$, and 639 mAh $g_{Tin}^{-1}$, respectively, throughout the 10 cycles. A comparison of the average desodiation capacity up to the tenth cycle revealed a notable difference between the two electrolytes. The conventional electrolyte exhibited an average desodiation capacity of ≈67 mAh $g_{Tin}^{-1}$, whereas that of the Na-Pyr electrolyte was almost ten-fold higher at 643 mAh $g_{Tin}^{-1}$ (Figure 2f). This indicates that the expansion of the tin structure during the charging process impeded charge transfer in the conventional electrolyte, leading to limited and extremely low capacity during desodiation. However, this issue was not observed in the Na-Pyr redox-mediator electrolytes, which demonstrated stable and reversible performance throughout the cycles.

### 2.3. Vertically Arranged Tin Electrode and Na-Pyr Redox-Mediator Electrolyte in SWBs

We investigated the effectiveness of a Na-Pyr redox-mediated electrolyte in enhancing the cyclability of vertically arranged tin electrodes, with the objective of improving energy density in SWBs. The tin electrodes were cut to dimensions of 3 mm × 14 mm and placed in either a horizontal orientation (left illustration in **Figure 3**a; Figure S7a, Supporting Information), a vertical orientation with conventional electrolyte (center illustration in Figure 3a; Figure S7b,c, Supporting Information), or a vertical orientation with Na-Pyr redox-mediator electrolyte (right illustration in Figure 3a). The horizontally oriented tin electrode showed an improvement in Coulombic efficiency from 40.6% in the first cycle to 91.2% in the third cycle (Figure 3b). On the other hand, the tin electrode placed vertically had a significantly lower Coulombic efficiency of 8.7% in the first cycle, which only improved to 14.6% in the third cycle (Figure 3c). The lack of charge transfer between electrically isolated tin particles, caused by the significant volume changes and pulverization of alloy-type anode materials such as tin during charging and discharging, results in detachment of the tin active material from the current collector. Upon investigation of the subsequent cycles (Figure S8, Supporting Information), it is evident that the desodiation of tin does not occur as expected. Instead, the plating and stripping reactions of sodium metal are dominant. This behavior is in clear contrast with the charge/discharge profiles of tin depicted in Figure 3b. As shown in Figure S9 (Supporting Information), tin that becomes disconnected from the current collector and electrically inactive cannot contribute to the overall capacity. This was additionally substantiated through SEM coupled with energy-dispersive X-ray spectroscopy (EDS) measurements of the electrode following the cycling process (Figure S9c–e, Supporting Information). These measurements revealed the presence of regions where tin particles had falling off, resulting in the exposure of the underlying copper foil. The vertical electrode structure exacerbates this issue, as it fails to physically maintain the structure and compress the pulverized tin particles. Figure 3d demonstrates the ability of the Na-Pyr redox mediator electrolyte to facilitate electron transfer between electrically isolated pulverized tin particles through the redox reaction of Na-Pyr. This resulted in Coulombic efficiency of 39.2% in the first cycle and 93.6% in the third cycle, which is comparable to that of a horizontal tin electrode. To evaluate the surface of the tin electrode when using the Na-Pyr redox mediator electrolyte, the electrode surface was examined through an SEM-EDS analysis conducted after the cycling (Figure S9f–h, Supporting Information). In contrast with the observations made with the conventional electrolyte, the SEM images revealed a uniform surface, which was further corroborated by the EDS analysis. In addition, when comparing the voltage profiles up to the third cycle, the vertically oriented tin electrode with the Na-Pyr redox-mediator electrolyte exhibited almost identical electrochemical behavior to the horizontally oriented tin electrode (Figure S10, Supporting Information). The vertically arranged tin electrode exhibited reversible charging and discharging capabilities for up to 400 cycles when combined with the Na-Pyr redox-mediator electrolyte (Figure 3e).

### 2.4. Morphological and Crystallographic Structure Analysis

In order to investigate whether the Na-Pyr redox mediator influenced the reversibility of the tin electrode, further experiments were conducted using SWB coin cells. These cells were

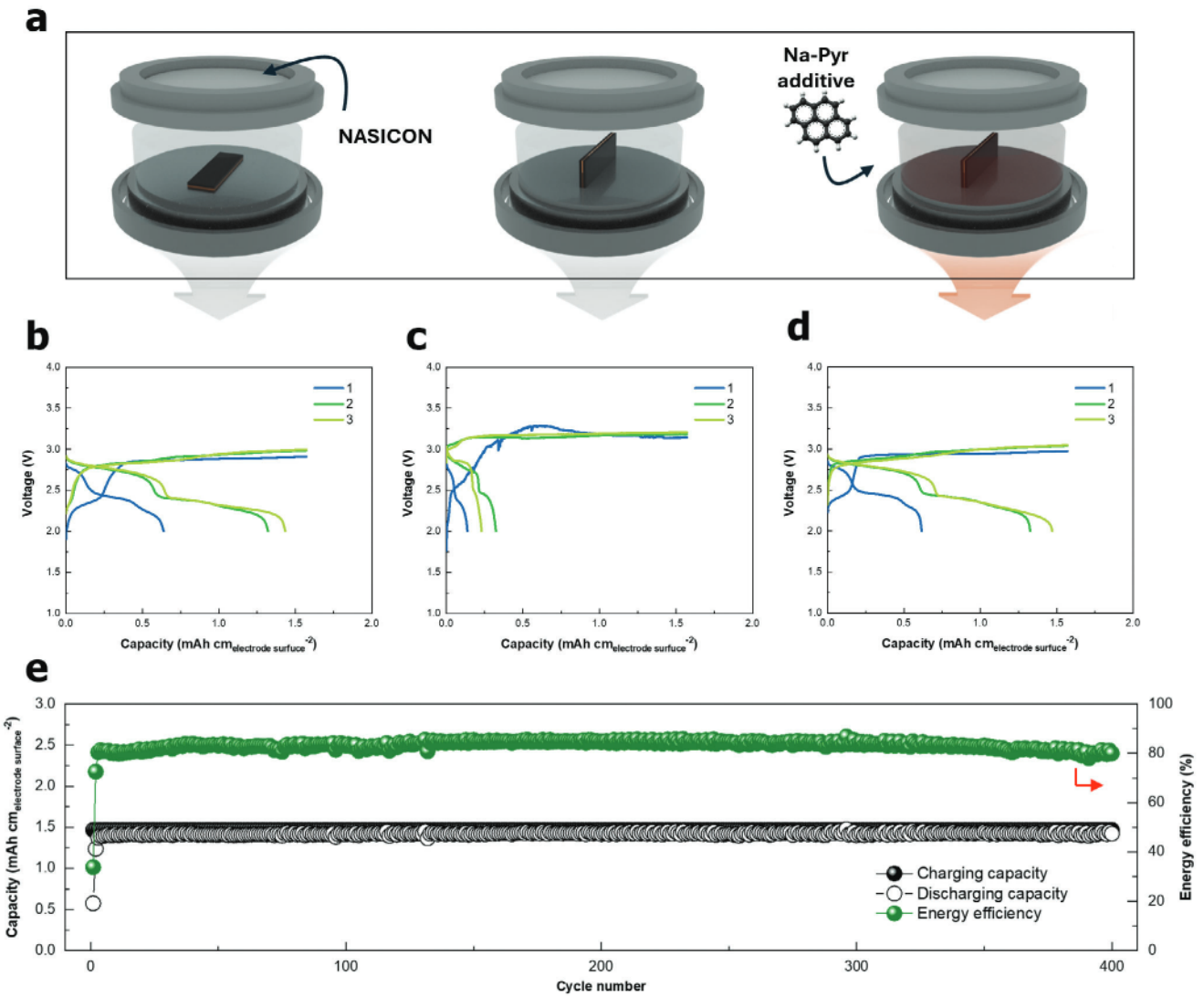


**Figure 3.** a) SWB coin cell design to verify the cyclability of the vertical tin electrode with a Na-Pyr redox-mediator electrolyte. The left illustration demonstrates a conventional electrolyte with a horizontal tin electrode, the center illustration demonstrates a conventional electrolyte with a vertical tin electrode, and the right illustration demonstrates a Na-Pyr redox-mediator electrolyte with a vertical tin electrode. b–d) Respective voltage profiles measured at a current density of 0.3 mA $cm^{-2}$. e) Cycle stability of vertical tin electrode with Na-Pyr redox-mediator electrolyte at the current density of 0.3 mA $cm^{-2}$.

assembled with conventional electrolyte or the Na-Pyr redox-mediator electrolyte. To analyze the morphology of the electrode surfaces, the cells were operated for 10 cycles at a current density of 0.3 mA $cm^{-2}$ and then discharged at the same current density. A rough surface was observed on the tin electrode using conventional electrolyte after 10 charge–discharge cycles (**Figure** 4a). This is attributed to the electrically isolated tin, which becomes pulverized and expands in volume due to sodiation during charging, being unable to undergo desodiation during discharge. Consequently, the electrode structure becomes compromised during subsequent charging cycles, as reflected in the charge–discharge voltage profile and Coulombic efficiency shown in Figure 3c. In contrast, the tin electrode with the Na-Pyr redox-mediator electrolyte maintained a smooth surface even after 10 charge–discharge cycles (Figure 4b). This indicates that the electrically isolated tin particles, which become separated upon sodiation during the charging process, are able to undergo desodiation through the redox reaction of Na-Pyr during the discharging process, thereby reversibly maintaining the electrode structure. This is also consistent with the voltage profile and Coulombic efficiency presented in Figure 3d,e.

The XRD analysis confirmed the sodiation and desodiation characteristics of the conventional or Na-Pyr redox-mediator electrolytes with vertical tin electrodes. During the sodiation process to 0 V and the subsequent desodiation to 1 V, changes in the XRD peaks on the electrode surface were monitored in situ using a half-cell with a conventional electrolyte (Figure 4c). As the sodiation capacity increased, additional peaks were observed at 32.1- and 35.0-degrees, indicating the formation of $Na_{15}Sn_4$ crystals during the sodiation process of the tin electrode.[32]

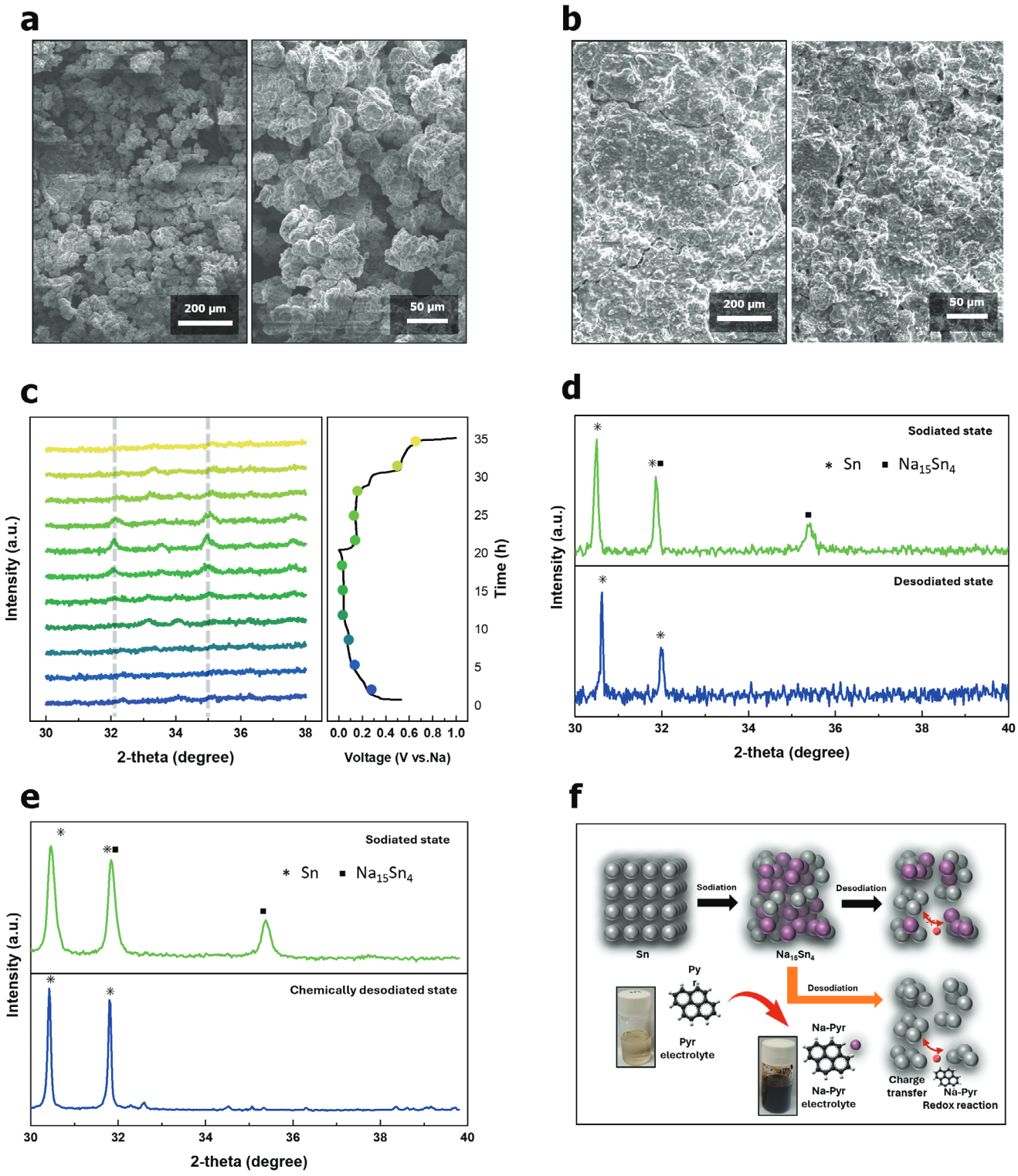


**Figure 4.** SEM images confirming the morphology of the electrode surface after 10 sodiation–desodiation cycles of the tin electrode with a) conventional electrolyte and b) Na-Pyr redox-mediator electrolyte at a current density of 0.3 mA $cm^{-2}$. c) In situ XRD measurements of the half-cell structure of the vertical tin electrode with conventional electrolyte in the 30–38-degree range, with voltage profiles during sodiation–desodiation where each sodiated state is indicated by the same color as the corresponding XRD peaks. d) Ex situ XRD peaks of vertically arranged tin electrode with Na-Pyr redox-mediator electrolyte. e) Ex situ XRD peaks of the sodiated tin electrode and the tin electrode immersed in Pyr electrolyte for 24 h. f) The schematic illustration that Na-Pyr could desodiation the electrically isolated tin particles.

During the subsequent desodiation process, these two peaks disappeared. Additionally, the weak peaks that appear and disappear at 33.2- and 34.0-degrees during the sodiation and desodiation processes correspond to intermediate intermetallic phases of Na–Sn, which is consistent with previous studies.[32] Figure 4d shows ex situ XRD observations of the vertical electrode following ten cycles of sodiation and desodiation. These measurements were conducted on a vertical tin electrode using an electrolyte containing the Na-Pyr redox mediator. In the sodiated state, the XRD peaks in the 30–40-degree range exhibited both tin (Sn) 30.6- and 32.0-degrees peaks and sodiated tin 32.0- and 35.4-degrees peaks ($Na_{15}Sn_4$). However, following desodiation, only the tin peaks at 30.6- and 32.0-degrees remained, while the sodiated tin peak at 35.4-degrees disappeared. This suggests that during the discharge process, the vertical tin electrode can be fully desodiated through the redox reaction of the Na-Pyr redox mediator. To further evaluate whether desodiation of the tin electrode could be achieved solely through the potential difference induced by the Pyr redox mediator, we investigated the spontaneous chemical desodiation of a tin electrode sodiated to 0 V at a current density of 0.19 mA $cm^{-2}$. The electrode was immersed in Pyr electrolyte, which contained no sodium source, for 24 h to observe whether spontaneous chemical desodiation would occur. Figure 4e displays the XRD peaks of the sodiated tin electrode and the tin electrode immersed in Pyr electrolyte for 24 h. The XRD peaks of the sodiated tin electrode clearly showed a $Na_{15}Sn_4$ peak at 35.4-degrees. This peak was absent after immersion in the Pyr electrolyte supporting for the complete chemical desodiation. The findings are depicted in the scheme in Figure 4f. In the presence of a conventional electrolyte, desodiation of the sodiated tin electrode was hindered due to electrically isolated tin particles by pulverization. However, with the use of a Na-Pyr redox mediator electrolyte, Na-Pyr itself facilitated the desodiation of the electrically isolated sodiated tin, thereby enabling the complete desodiation.

### 2.5. Estimation of Charge Transfer Resistance via Impedance Spectroscopy

Electrochemical impedance spectroscopy (EIS) was utilized to evaluate the charge transfer resistance between the tin electrode and the conventional electrolyte, as well as between the tin electrode and the Na-Pyr redox-mediator electrolyte. To characterize the charge transfer resistance between the tin electrode and the electrolytes, a symmetric cell was fabricated, and the frequency and capacitance of the Nyquist plot for each element and interface of the complete cell were determined (Figure S11 and Table S2, Supporting Information). Looking at the EIS measurements of the NASICON solid electrolyte (Figure S11a, Supporting Information) and the Na-Pyr electrolyte (Figure S11b, Supporting Information) cells, which consist of coated Pt and SUS as both electrodes, the frequency at the maximum was determined to be 1.04 MHz and 7700 Hz, respectively. To ascertain the frequency and capacitance associated with charge transfer between the Na metal electrode and the conventional electrolyte in a half-cell with Na metal as the counter electrode, a cell was constructed with structure Na | CE | Na, yielding a frequency at the maximum of 10 kHz (Figure S11d, Supporting Information). Furthermore, to ascertain the frequency and capacitance of the SEI layer on the Na metal electrode during the cycle, a SEI layer was formed on the Na metal electrode by charging and discharging for 10 h at a current density of 100 μA $cm^{-2}$ (denoted as A. Na). Subsequently, cells with the structures A. Na | CE | A. Na and A. Na | CE | NASICON | CE | A. Na were assembled. EIS measurements indicated that the maximum frequency of interfacial resistance between the Na metal electrode and the conventional electrolyte was 19 kHz, while the frequency of charge transfer resistance between the conventional electrolyte and NASICON was 480 Hz (Figure S11e,f, Supporting Information). Similarly, EIS was employed to assess the maximum frequency of interfacial and charge transfer resistance of a tin electrode in cells with the structure A. Tin | CE | A. Tin and A. Tin | CE | NASICON | CE | A. Tin, after 15 h of charging and discharging at a current of 100 μA $cm^{-2}$ (equivalent to 50% of the state of charge). The maximum frequency of the interfacial and charge transfer features between the tin electrode and the conventional electrolyte were determined to be 130 kHz and 810 Hz, respectively. Additionally, the maximum frequency of the charge transfer resistance between the conventional electrolyte and NASICON was ascertained to be 1100 Hz (Figure S11g,h, Supporting Information). Finally, to ascertain the capacitance associated with the Pyr electrolyte, cells with the following structures were constructed: SUS | Pyr | NASICON | Pyr | SUS and A. Tin | Pyr | NASICON | Pyr | A. Tin. The maximum frequency of the charge transfer resistance between the Na-Pyr redox-mediator electrolyte and NASICON was determined to be 2500 Hz, whereas that between the tin electrode and the Na-Pyr redox-mediator electrolyte was determined to be 1500 Hz (Figure S11i,j, Supporting Information).

A half-cell with Na metal as the counter electrode and a SWB half-cell with sodium ferrocyanide as the counter electrode were prepared based on the measured frequency and capacitance. The charge transfer to the tin electrode and electrolytes was estimated on a cycle-by-cycle basis. Charging and discharging were conducted at a current density of 0.19 mA $cm^{-2}$, and EIS measurements were taken before cycling and after each cycle up to the fifth cycle. In the half-cell with Na metal as the counter electrode, the combination of conventional electrolyte and tin electrode (**Figure 5a**; Figure S12a, Supporting Information) demonstrated initial activation of the electrode, with the charge transfer resistance decreasing from 198 Ω before cycling to 15.6 Ω after the first cycle. However, the charge transfer resistance subsequently increased to 20.4 Ω after the fifth cycle (Figure 5c). In contrast, the combination of the Na-Pyr redox-mediator electrolyte and tin electrode (Figure 5b; Figure S12b, Supporting Information) demonstrated a charge transfer resistance of 3.43 Ω after the first cycle, representing a decrease from 18.8 Ω prior to cycling. This resistance further decreased to 2.75 Ω following the fifth cycle (Figure 5c). Furthermore, in the SWB half-cell with sodium ferrocyanide as the counter electrode, the combination of the conventional electrolyte and tin electrode (Figure 5d; Figure S12c, Supporting Information) demonstrated a reduction in charge transfer resistance from 260 Ω before cycling to 24.4 Ω after the first cycle, followed by an increase to 29.2 Ω after the fifth cycle (Figure 5f). On the other hand, the combination with the Na-Pyr redox-mediator (Figure 5e; Figure S12d, Supporting Information) exhibited a decrease in resistance from 10.7 Ω before cycling to 8.0 Ω after the first cycle, which further reduced

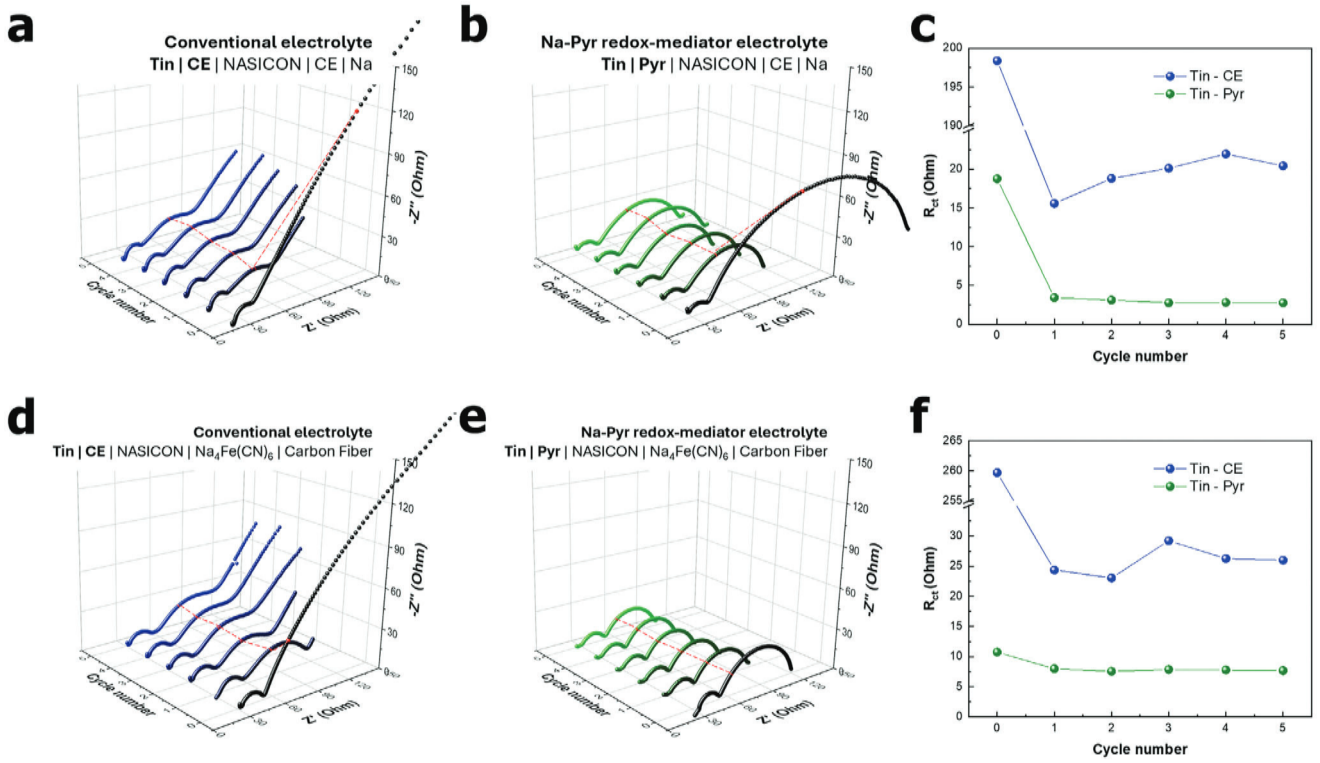


**Figure 5.** EIS measurement results during charging and discharging cycles at a current density of 0.19 mA $cm^{-2}$. For the half-cell with Na metal foil as the counter electrode and tin electrode: a) combination with conventional electrolyte and b) with Na-Pyr redox-mediator electrolyte. The frequency corresponding to the charge transfer resistance is indicated by a red dot line, as well as c) the estimated charge transfer resistance between the tin electrode and electrolytes. For the SWB half-cell with sodium ferrocyanide as the counter electrode and tin electrode: d) combination with conventional electrolyte and e) with Na-Pyr redox-mediator electrolyte. The frequency corresponding to the charge transfer resistance is indicated by a red dot line, as well as f) the estimated charge transfer resistance between the tin electrode and electrolytes.

to 7.70 Ω after the fifth cycle (Figure 5f). By the fifth cycle of the seawater battery, the utilization of the Na-Pyr redox mediator electrolyte has been observed to reduce the charge transfer resistance between the electrolyte and the tin electrode by 73.6%. In previous density functional theory study,[21] it was observed that incorporating a redox mediator alongside the conventional electrolyte salt facilitated electron accommodation due to the $\pi$ system of the redox mediator. This resulted in a reduction in charge transfer resistance and an increase in $Na^+$ ion conductivity. These findings are consistent with the results of this study, where the use of the Na-Pyr redox mediator effectively reduced the charge transfer resistance between the tin electrode and the electrolyte.

### 2.6. Maximizing Areal Capacity by Combining a Vertically Arranged Tin Electrode with Na-Pyr Redox-Mediator Electrolyte

The previous studies confirmed that the combination of Na-Pyr redox-mediator electrolyte and vertically arranged tin electrodes can achieve high reversibility. In order to push the cell optimization further, the potential for achieving high areal capacity by arranging the vertical tin electrodes within a specific area in a seawater coin cell is also investigated (Figure S14a, Supporting Information). The tin electrode was slit to dimensions of 3 mm × 360 mm and wounded in a spiral arrangement as shown in Figure S14b (Supporting Information). The seawater half-cell system, using sodium ferrocyanide as the catholyte, achieved a capacity of 6 mAh $cm^{-2}$ (equivalent to 12 mAh) when operated at a current density of 0.3 mA $cm^{-2}$. The charging voltage was ≈3.0 V, while the discharging voltage was 2.4 V (**Figure 6a**). During the cyclability test, the system demonstrated reliable operation for >80 cycles, as shown in Figure 6b. By increasing the electrode dimensions to 3 mm × 600 mm in the seawater coin cell, the system was evaluated under the same current density conditions and successfully achieved a capacity of 10 mAh $cm^{-2}$ (20 mAh) while maintaining stable performance for over 40 cycles (Figure 6c). In addition, by maximizing the electrode array to a size of 3 mm × 2400 mm within the allotted area and performing galvanostatic charging–discharging at a current density of 0.3 mA $cm^{-2}$, stable operation for >20 cycles was demonstrated. Throughout the operation, Coulombic efficiency averaged 94.6%, while energy efficiency averaged 79.5% (Figure 6d). This study demonstrates that areal capacity can be optimized by vertically arranging tin electrodes with inherent high energy density, and that high reversibility can be achieved by utilizing a Na-Pyr redox-mediator electrolyte. These results highlight the potential to significantly enhance the energy storage capacity of seawater battery systems, representing a pivotal step toward their practical application as energy storage devices.

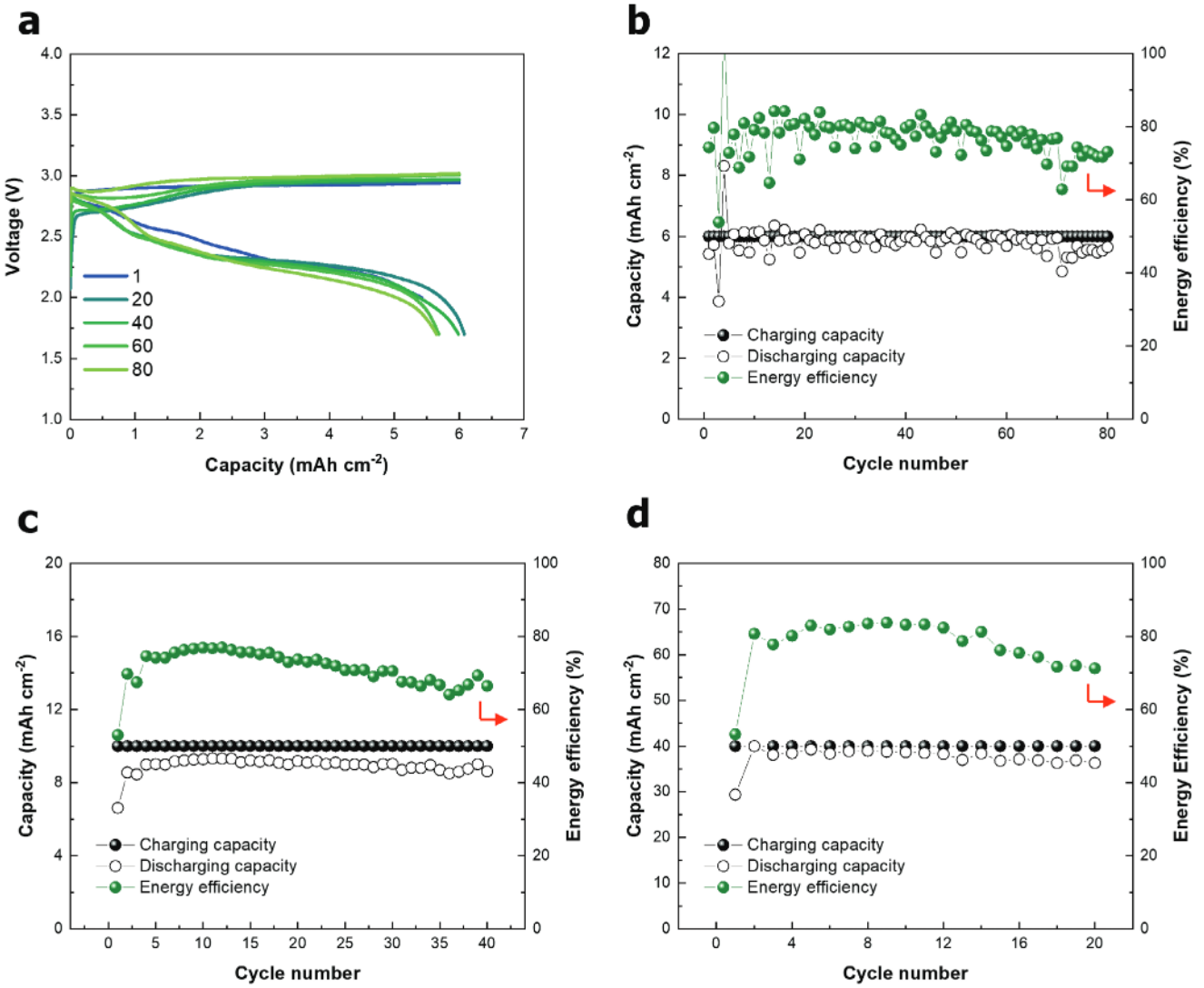


**Figure 6.** a) Voltage profile and b) cyclability of a vertical tin electrode and Na-Pyr redox-mediator electrolyte applied to a seawater battery with an areal capacity of 6 mAh $cm^{-2}$. c) Cyclability with an areal capacity of 10 mAh $cm^{-2}$. d) Cyclability with an areal capacity of 40 mAh $cm^{-2}$. All charging and discharging cycles were conducted at a current density of 0.3 mA $cm^{-2}$.

## 3. Conclusion

The aim of this study was to enhance the energy density of the anode in a seawater battery, by employing vertically arranged micro-sized tin electrodes and a Na-pyrene redox-mediator electrolyte. In this study, the introduction of pyrene as a redox mediator, which matches the redox potential of tin, enabled effective charge transfer to electrically isolated tin particles via the redox reaction of Na-Pyr, thereby improving reversibility by avoiding issues related to the pulverization and electrical isolation of tin particles during cycling. The charge transfer reaction between tin and the Na-Pyr redox-mediator electrolyte, investigated using EIS, is demonstrated to maintain lower values than with the conventional electrolyte. The Na-Pyr redox mediator enables high capacity and reversibility in vertically arranged tin electrodes, which achieve a capacity of 6 mAh $cm^{-2}$ for, at least, 80 cycles. As a proof of scale-ability, reversible operation at 40 mAh $cm^{-2}$ was also demonstrated with the vertically arranged tin electrode design. This approach shows significant promise for increasing the energy density of electrodes in battery systems using solid electrolytes and membranes, including not only seawater batteries but also solid-state batteries, metal–air batteries, and similar systems.

## 4. Experimental Section

*Preparation of Materials*: The conventional electrolyte was made with a composition of 1 M $NaPF_6$ in DEGDME. The 0.5 M Na-Pyr redox-mediator electrolyte was prepared by the following process. First, 10.1 g of Pyr (0.05 mol, Sigma–Aldrich) and 16.80 g of $NaPF_6$ (0.1 mol, Alfa Aesar) were dissolved in DEGDME to a total volume of 100 ml. Then, 3.45 g of Na metal was chopped and added to the solution. The electrolyte was prepared by stirring for over 24 h. All the above processes were performed in a glove box in an Ar atmosphere where moisture and oxygen were limited ($H_2O$ < 0.1 ppm, $O_2$ < 0.1 ppm). To prepare the tin electrode, a slurry containing

85% tin (Alfa Aesar) as the active material, 5% carbon black (Super-P), 5% polyacrylic acid (Meishan Indigo), and 5% carboxymethylcellulose sodium (Sigma–Aldrich) was contained in distilled water. The slurry was coated onto a copper foil current collector with a loading of ≈5.5 mg $cm^{-2}$. The electrode was then dried in an oven at 80 °C under vacuum overnight.

*Characterization*: The electronic and ionic conductivity of the Na-Pyr redox-mediator electrolyte was calculated using the isothermal transient ionic current (ITIC) method. Stainless steel electrodes were placed on both sides of the electrolyte, and the current curve was also measured while applying 0.1 V voltage. The measured current values provided data on the electronic and ionic conductivity of the Na-Pyr redox-mediator electrolyte. Ex situ X-ray diffraction (XRD) analysis was conducted using a D/MAX2500V/PC (Rigaku) equipped with an 18 kW Cu rotating anode X-ray source to investigate the sodiation and desodiation states of the tin electrode. The scan range was set from 20° to 50° at a scan rate of 0.5°/min. In situ XRD was conducted using an Empyrean diffractometer (Malvern Panalytical) at the Korea Basic Science Institute (KBSI). The customized cell was designed and assembled for characterization, and a Be window was used for penetration of X-ray into the cell during charge–discharge.

*Electrochemical Measurements*: The coin-cell used in the experiment was produced by purchasing SWB 2464 coin-cell parts from 4toOne. As the catholyte material for the SWB half-cell test, 0.4 M of sodium ferrocyanide decahydrate (Thermo Fisher Scientific Inc., Republic of Korea) dissolved in natural seawater (Ilsan beach, Ulsan, Republic of Korea (GPS: 35.497005, 129.430996)) without filtration. Carbon fiber (dimensions 4 cm × 4 cm) was used as the current collector and held in position by a titanium mesh. A WBCS3000 battery cycler (Wonatech) was used for galvanostatic charging and discharging. The current density was 0.3 mA $cm^{-2}$, based on the area of the NASICON in the seawater battery. Electrochemical impedance spectroscopy was performed after allowing sufficient time for each cell to reach stabilization. The measurements were conducted using a VSP-300 multichannel potentiostat/galvanostat (Biologic), with a frequency range of 7 MHz to 1 Hz with an amplitude of 10 mV.

## Acknowledgements

D.K., Y.J., and W.-G.L. contributed equally to this work. This work was supported by the Technology Innovation Program funded by the Korea government (MOTIE) (No. RS-2024-00409090).

## Conflict of Interest

The authors declare no conflict of interest.

## Data Availability Statement

The data that support the findings of this study are available from the corresponding author upon reasonable request.

## Keywords

battery electrode architecture, pyrene, redox mediator, seawater batteries, sodium-ion batteries, tin, vertical electrode

[1] a) K. C. Divya, J. Østergaard, *Electr. Power Syst. Res.* **2009**, *79*, 511; b) G. G. Njema, R. B. O. Ouma, J. K. Kibet, *J. Renew. Energy* **2024**, *2024*, 2329261.

[2] a) S. Manzetti, F. Mariasiu, *Renew. Sust. Energ. Rev.* **2015**, *51*, 1004; b) G. Zubi, R. Dufo-López, M. Carvalho, G. Pasaoglu, *Renew. Sust. Energ. Rev.* **2018**, *89*, 292; c) M. Armand, P. Axmann, D. Bresser, M. Copley, K. Edström, C. Ekberg, D. Guyomard, B. Lestriez, P. Novák, M. Petranikova, W. Porcher, S. Trabesinger, M. Wohlfahrt-Mehrens, H. Zhang, *J. Power Sources* **2020**, *479*, 228708; d) M. Li, J. Lu, Z. Chen, K. Amine, *Adv. Mater.* **2018**, *30*, 1800561.

[3] a) T. L. Kulova, V. N. Fateev, E. A. Seregina, A. S. Grigoriev, *Int. J. Electrochem. Sci.* **2020**, *15*, 7242; b) S. Choi, G. Wang, *Adv. Mater. Technol.* **2018**, *3*, 1700376; c) G. E. Blomgren, *J. Electrochem. Soc.* **2017**, *164*, A5019.

[4] a) J.-K. Kim, E. Lee, H. Kim, C. Johnson, J. Cho, Y. Kim, *ChemElectroChem* **2015**, *2*, 328; b) S. M. Hwang, J.-S. Park, Y. Kim, W. Go, J. Han, Y. Kim, Y. Kim, *Adv. Mater.* **2019**, *31*, 1804936.

[5] a) J. Bae, H. Bae, J. Cho, J. Jung, Y. Choi, Y. Kim, *J. Mater. Chem. A* **2022**, *10*, 6481; b) J. Bae, Y. Choi, Y. Kim, *Energies* **2024**, *17*, 2418.

[6] S. T. Senthilkumar, W. Go, J. Han, L. Pham Thi Thuy, K. Kishor, Y. Kim, Y. Kim, *J. Mater. Chem. A* **2019**, *7*, 22803.

[7] a) J. Han, S. Lee, C. Youn, J. Lee, Y. Kim, T. Choi, *Electrochim. Acta* **2020**, *332*, 135443; b) W. Lee, J. Park, J. Park, S. J. Kang, Y. Choi, Y. Kim, *J. Mater. Chem. A* **2020**, *8*, 9185; c) J. Park, J.-S. Park, S. T. Senthilkumar, Y. Kim, *J. Power Sources* **2020**, *450*, 227600.

[8] a) W. Go, J. Kim, J. Pyo, J. B. Wolfenstine, Y. Kim, *ACS Appl. Mater. Interfaces* **2021**, *13*, 52727; b) W. Go, Y. Kim, *ECS Meeting Abstracts* **2019**, *02*, 567; c) Y. Kim, H. Kim, S. Park, I. Seo, Y. Kim, *Electrochim. Acta* **2016**, *191*, 1; d) M. Li, M. Dixit, R. Essehli, C. J. Jafta, R. Amin, M. Balasubramanian, I. Belharouak, *Adv. Sci.* **2023**, *10*, 2300920; e) T.-U. Wi, C. Lee, F. Rahman, W. Go, M.-H. Kim, S. H. Kim, D. Hwang, S. K. Kwak, Y. Kim, H.-W. Lee, *ECS Meeting Abstracts* **2019**, *02*, 73.

[9] J. Han, S. M. Hwang, W. Go, S. T. Senthilkumar, D. Jeon, Y. Kim, *J. Power Sources* **2018**, *374*, 24.

[10] a) L. Sun, Y. Liu, R. Shao, J. Wu, R. Jiang, Z. Jin, *Energy Stor. Mater.* **2022**, *46*, 482; b) Y. Kim, Y. Park, A. Choi, N.-S. Choi, J. Kim, J. Lee, J. H. Ryu, S. M. Oh, K. T. Lee, *Adv. Mater.* **2013**, *25*, 3045.

[11] a) D. J. Arnot, K. S. Mayilvahanan, Z. Hui, K. J. Takeuchi, A. C. Marschilok, D. C. Bock, L. Wang, A. C. West, E. S. Takeuchi, *Acc. Chem. Res.* **2022**, *3*, 472; b) Y. Kuang, C. Chen, D. Kirsch, L. Hu, *Adv. Energy Mater.* **2019**, *9*, 1901457.

[12] a) Y. Kim, S. M. Hwang, H. Yu, Y. Kim, *J. Mater. Chem. A* **2018**, *6*, 3046; b) I. Capone, J. Aspinall, E. Darnbrough, Y. Zhao, T.-U. Wi, H.-W. Lee, M. Pasta, *Matter* **2020**, *3*, 2012; c) G. Chu, B.-N. Liu, F. Luo, W.-J. Li, H. Lu, L.-Q. Chen, H. Li, *Chin. Phys. B* **2017**, *26*, 078201; d) Y. Liu, Q. Liu, C. Jian, D. Cui, M. Chen, Z. Li, T. Li, T. Nilges, K. He, Z. Jia, C. Zhou, *Nat. Commun.* **2020**, *11*, 2520.

[13] a) X. Wu, X. Lan, R. Hu, Y. Yao, Y. Yu, M. Zhu, *Adv. Mater.* **2022**, *34*, 2106895; b) H. Mou, W. Xiao, C. Miao, R. Li, L. Yu, *Front. Chem.* **2020**, *8*, 141; c) Z. Li, J. Ding, D. Mitlin, *Acc. Chem. Res.* **2015**, *48*, 1657.

[14] a) S.-M. Zheng, Y.-R. Tian, Y.-X. Liu, S. Wang, C.-Q. Hu, B. Wang, K.-M. Wang, *Rare Met.* **2021**, *40*, 272; b) H. Li, T. Yamaguchi, S. Matsumoto, H. Hoshikawa, T. Kumagai, N. L. Okamoto, T. Ichitsubo, *Nat. Commun.* **2020**, *11*, 1584.

[15] H. Wu, Y. Cui, *Nano Today* **2012**, *7*, 414.

[16] a) H. Haftbaradaran, X. Xiao, M. W. Verbrugge, H. Gao, *J. Power Sources* **2012**, *206*, 357; b) B. Lu, Y. Song, J. Zhang, *J. Power Sources* **2015**, *289*, 168; c) Y. B. Sim, B. K. Park, K. J. Kim, *Front. Batter. Electrochem.* **2023**, *2*, 1272439.

[17] a) J. G. Werner, G. G. Rodríguez-Calero, H. D. Abruña, U. Wiesner, *Energy Environ. Sci.* **2018**, *11*, 1261; b) K. Sun, T.-S. Wei, B. Y. Ahn, J. Y. Seo, S. J. Dillon, J. A. Lewis, *Adv. Mater.* **2013**, *25*, 4539; c) J. S. Sander, R. M. Erb, L. Li, A. Gurijala, Y. M. Chiang, *Nat. Energy* **2016**, *1*, 16099; d) C. Chen, Y. Zhang, Y. Li, Y. Kuang, J. Song, W. Luo, Y. Wang,

Y. Yao, G. Pastel, J. Xie, L. Hu, *Adv. Energy Mater.* **2017**, *7*, 1700595. e) J. Billaud, F. Bouville, T. Magrini, C. Villevieille, A. R. Studart, *Nat. Energy* **2016**, *1*, 16097.

[18] a) T.-S. Wei, B. Y. Ahn, J. Grotto, J. A. Lewis, *Adv. Mater.* **2018**, *30*, 1703027; b) J. Hu, Y. Jiang, S. Cui, Y. Duan, T. Liu, H. Guo, L. Lin, Y. Lin, J. Zheng, K. Amine, F. Pan, *Adv. Energy Mater.* **2016**, *6*, 1600856; c) K. Fu, Y. Yao, J. Dai, L. Hu, *Adv. Mater.* **2017**, *29*, 1603486; d) K. Fu, Y. Wang, C. Yan, Y. Yao, Y. Chen, J. Dai, S. Lacey, Y. Wang, J. Wan, T. Li, Z. Wang, Y. Xu, L. Hu, *Adv. Mater.* **2016**, *28*, 2587.

[19] Y. Jung, S. Lee, D. Kim, H. Lee, S. Kim, J. Cho, H. Jin, Y. Kim, J.-S. Park, W.-G. Lee, *J. Power Sources* **2024**, *592*, 233960.

[20] a) C. M. Wong, C. S. Sevov, *ACS Energy Lett.* **2021**, *6*, 1271; b) J.-B. Park, S. H. Lee, H.-G. Jung, D. Aurbach, Y.-K. Sun, *Adv. Mater.* **2018**, *30*, 1704162; c) E. C. Self, F. M. Delnick, R. E. Ruther, S. Allu, J. Nanda, *ACS Energy Lett.* **2019**, *4*, 2593; d) Y. Kim, A. Varzi, A. Mariani, G.-T. Kim, Y. Kim, S. Passerini, *Adv. Energy Mater.* **2021**, *11*, 2102061.

[21] Y. Kim, A. Varzi, A. Mariani, G.-T. Kim, Y. Kim, S. Passerini, *Adv. Energy Mater.* **2021**, *11*, 2102061.

[22] G. Wang, B. Huang, D. Liu, D. Zheng, J. Harris, J. Xue, D. Qu, *J. Mater. Chem. A* **2018**, *6*, 13286.

[23] a) T. A. Baker, M. Head-Gordon, *J. Phys. Chem. A* **2010**, *114*, 10326; b) M. Liu, J. Zhang, S. Guo, B. Wang, Y. Shen, X. Ai, H. Yang, J. Qian, *ACS Appl. Mater. Interfaces* **2020**, *12*, 17620.

[24] a) P. Barnes, K. Smith, R. Parrish, C. Jones, P. Skinner, E. Storch, Q. White, C. Deng, D. Karsann, M. L. Lau, J. J. Dumais, E. J. Dufek, H. Xiong, *J. Power Sources* **2020**, *447*, 227363; b) F. Cheng, M. Cao, Q. Li, C. Fang, J. Han, Y. Huang, *ACS Nano* **2023**, *17*, 18608.

[25] a) H. Pan, X. Lu, X. Yu, Y.-S. Hu, H. Li, X.-Q. Yang, L. Chen, *Adv. Energy Mater.* **2013**, *3*, 1186; b) Y. Kim, J. Jung, H. Yu, G.-T. Kim, D. Jeong, D. Bresser, S. J. Kang, Y. Kim, S. Passerini, *Adv. Funct. Mater.* **2020**, *30*, 2001249; c) G. Chu, B.-N. Liu, F. Luo, W.-J. Li, H. Lu, L.-Q. Chen, H. Li, *Chin. Phys. B* **2017**, *26*, 078201.

[26] D. Kim, J.-S. Park, W.-G. Lee, Y. Choi, Y. Kim, *J. Electrochem. Soc.* **2022**, *169*, 040508.

[27] a) C.-C. Chang, S.-J. Liu, J.-J. Wu, C.-H. Yang, *J. Phys. Chem. C* **2007**, *111*, 16423; b) M. O. Guler, M. Guzeler, D. Nalci, M. Singil, E. Alkan, M. Dogan, A. Guler, H. Akbulut, *Appl. Surf. Sci.* **2018**, *446*, 122; c) J.-M. Liang, L.-J. Zhang, D.-G. XiLi, J. Kang, *Rare Met.* **2020**, *39*, 1005; d) B. Luo, T. Qiu, D. Ye, L. Wang, L. Zhi, *Nano Energy* **2016**, *22*, 232.

[28] L. Sun, Y. Liu, L. Wang, Z. Jin, *Adv. Funct. Mater.* **2024**, *34*, 2403032.

[29] A. Daali, R. Amine, W. Otieno, G.-L. Xu, K. Amine, *Ind. Chem. Mater.* **2024**, *2*, 489.

[30] a) H. Mou, W. Xiao, C. Miao, R. Li, L. Yu, *Front. Chem.* **2020**, *8*, 141; b) X. Wu, X. Lan, R. Hu, Y. Yao, Y. Yu, M. Zhu, *Adv. Mater.* **2022**, *34*, 2106895.

[31] F. Dai, M. Cai, *Commun. Mater.* **2022**, *3*, 64.

[32] T. Palaniselvam, M. Goktas, B. Anothumakkool, Y.-N. Sun, R. Schmuch, L. Zhao, B.-H. Han, M. Winter, P. Adelhelm, *Adv. Funct. Mater.* **2019**, *29*, 1900790.